

Zinc oxide nano-crystals assisted for carbon dioxide gas sensing prepared by solvothermal and sonochemical methods

Mahdieh Ghobadifard, Qasem Maleki, Mostafa Khelghati, Ehsan Zamani, Saeid Farhadi*, Alireza Aslani

Department of Chemistry, University of Lorestan, Lorestan-Khoramabad 68135-465, Iran

Received: 2 June 2014, Accepted: 23 July 2014, Published: 1 October 2014

Abstract

ZnO nanostructures of different methods and sizes were grown in a controlled manner using a simple hydrothermal and sonochemical technique. Controlling the content of concentration and temperature of the reaction mixture, spherical nanoparticles ZnO structures could be synthesized at temperatures 100-150 °C with excellent reproducibility in solvothermal and at different power and time in sonochemical methods. These ZnO nanostructures have been tested for CO₂ gas monitoring by depositing them as thick films on an inter-digitated alumina substrate and evaluating the surface resistance of the deposited layer as a function of operating temperature and CO₂ concentrations. The gas sensitivity tests have demonstrated that the ZnO nanostructures, spherical morphology, exhibit high sensitivity to CO₂ proving their applicability in gas sensors. The role of the nanostructure on the sensing properties of ZnO is also discussed.

Keywords: ZnO; metal oxides; CO₂ gas sensor; sonochemistry.

Introduction

Metal oxides represent an assorted and appealing class of materials whose properties cover the entire range from metals to semiconductors and insulators and almost all aspects of material science and physics in areas including superconductivity and magnetism. In the field of chemical sensing, for more than five decades it has been known that the electrical conductivity of semiconductors varies with the composition of the gas atmosphere surrounding them. Gas sensors have a great influence in many areas such as environmental monitoring, domestic safety, public security, automotive

applications, air conditioning in airplanes, space crafts and houses and sensors networks. Due to this huge application range the need of cheap, small, low power consuming and reliable solid state gas sensors has grown over the years and triggered a huge research worldwide to overcome metal oxide sensors drawbacks, summed up in improving the well-known Sensitivity, Selectivity and Stability. The sensing properties of semiconductor metal oxide in form of thin or thick films other than SnO₂, like TiO₂, WO₃, ZnO, Fe₂O₃ and In₂O₃, have been studied as well as the benefits from the addition of noble

*Corresponding author: Saeid Farhadi

Tel: +98 (916) 6614530; Fax: +98 (661) 6200612

E-mail: sfarhadi48@yahoo.com

metals: Pd, Pt, Au and Ag in improving selectivity and stability. In 1991 Yamazoe [1] showed the reduction of sensor performance [2]. In a low grain size metal oxide almost all the carriers are trapped in surface states and only a few thermal activated carriers are available for conduction. In this configuration the transition from activated to strongly not activate carrier density, produced by target gases species, has a great effect on sensor conductance. The challenge became to prepare materials with small crystallize size which were stable when operated at high temperature for long periods[2]. From the preparation side, first generation devices were prepared by thick film technology starting from powders. Since sensor performance depends on percolation path of electrons through intergranular regions, by varying small details in the preparation process, each sensor differed slightly in its initial characteristics. Therefore, the materials fabrication processes have been improved towards thin film technology, a more automated production method that offers higher reproducibility and compatibility with Si technology, by physical and chemical vapors deposition. However, the technological improvement went along with a reduction of sensing performances due to a lower porosity of the prepared devices. Both thin and thick films electrical properties drift due to grain coalescence, porosity modification and grain-boundary alteration. These effects become more critical because the metal oxide layers must be kept at a relatively high temperature in order to guarantee the reversibility of chemical reactions at surface. Thus, several solutions have been put forward to stabilize the nanostructure, e.g. addition of a foreign element [3] or phase [4]. An

unexpected step forward has been the successful preparation of stable single crystal quasi-one-dimensional semiconducting oxides nanostructures (so-called nano-belts, nano-wires or nano-ribbons) by simply evaporating the desired commercial metal oxide powders at high temperatures [5,6]. Their crystallinity assures improved stability and the nanosized lateral dimension has good sensing properties. Their peculiar characteristics and size effects make them interesting both for fundamental studies and for potential nano-device applications, leading to a third generation of metal oxide gas sensors. On the other hand, Nano-materials are at the leading edge of rapidly developing field of nanotechnology [7-10]. A reduction in particle size to nanometer scale results in various special and interesting properties compared to their bulk properties. Metal oxide materials, specifically materials with nanoscale features, have been the subject of numerous research efforts in fields such as gas sensors [11,12], fuel cells [13], solar cells [14,15] and electrodes for lithium ion batteries [16] to name a few. However, ZnO is a polar inorganic crystalline material with many applications due to its unique combination of interesting properties such as non-toxicity, good electrical, optical and piezoelectric behavior, stability in a hydrogen plasma atmosphere and low price [17]. ZnO is a well-known semiconductor with a wide direct band gap (3.37 eV) and a large exciton binding energy of 60 meV at room temperature [18,19] and it has a wide range of applications such as solar cells, luminescent, electrical and acoustic devices, gas and chemical sensors, coatings, catalysts, micro lasers, memory arrays and biomedical applications [17,20]. Till now, many

methods have been developed to synthesize zinc oxide Nano crystals including vapor phase growth [21], vapor- liquid- solid process [22], soft chemical method [23], electrophoresis deposition [24], sol-gel process [25], and homogeneous precipitation [26-28]. Further works in a FET configuration have been reported on zinc oxide nanostructures. Fan *et al.* [29] reported oxygen adsorption on the nanowire surface. It was shown a considerable variation of electrical properties of the single crystal ZnO nanowire upon oxygen introduction. Furthermore, an interesting study of the response to oxygen as a function of the nanowire dimensions was reported, evidencing an increase in the response as the nanowire radius decreases. The same group in [30] characterized the electrical properties of ZnO nanowire field effect transistors with scanning probe microscopy. The potential drop at Schottky barrier contact was analyzed, the conductive SPM tip was used as a movable local gate in order to change the electrical properties of FET device. Finally, gas-sensing properties of ZnO single nanowire FET were tested towards NO₂ and NH₃ at room temperature [31]. As in the previous reported investigations, the electrical field applied to the back gate electrode influenced the sensitivity. A strong field was used to refresh the sensor after molecules adsorption at room temperature; the negative voltage pulse produced a complete recovery of the conductance value to the initial level before NO₂ exposure. The negative gate potential depleted electron in nano-wire and reduced the number of electrons available at the vacancy sites, the hole migration to the surface instead led to a discharge of gas molecules. Furthermore, if a dipole moment is associated with the adsorbed molecule,

the gate field can induce a repulsive field weakening the bonding. Some of the electrical measurement on nanowires gas sensors were carried out in ideal atmospheres, but clearly, if a gas sensing device has to be produced, more realistic condition have to be explored, air has to be used as a carrier gas and the effect of interfering gases and humidity have to be taken into account in the right concentration range. Nevertheless the presented experiments show good sensing properties, the possibility to use dopants and catalyze such in the thin film gas sensors and the real integration in low power consumption transducers of single crystalline nanobelts. The integration of top down and bottom up approaches prove the feasibility of large scale manufacturing of well-organized sensor arrays based on different nanostructures [2]. ZnO nanoparticles were synthesized by sonochemical method. In addition, the nanoparticles of ZnO were prepared by thermal oxidation on Zn substrate through importing the polycarbonate membrane template for initial deposition of Zn nuclei [32]. The above mentioned Methods cannot be departed from complex chemical reactions or processes. Thermal oxidation may assist the production of catalysts, semiconductor devices or functional oxide films under controlled conditions [33]. A direct and simple thermal oxidation method was employed to synthesize ZnO nanoparticles. Using this convenient route, with no catalyst and template assisted, many research teams prepared ZnO nanoparticles successfully by oxidizing zinc foils under different conditions such as different annealing temperatures, time or atmosphere [34-41]. X-ray diffraction (XRD), scanning electron microscopy (SEM), EDAX, Raman,

solid state UV-Vis and solid state PL spectra were used to characterize the morphology, structure and phase of the synthesized nanostructures. In the present work, we report data about their gas-sensing properties, by using them as active layers in CO₂ gas resistive sensors. The gas sensing properties of the different nanostructures were compared and discussed as a function of the morphology of the primary nanoparticles. The results presented highlighted the role of the shape of the primary ZnO crystallites and an explanation based on the characterization and sensing data acquired has been given.

Experimental

Sonochemical synthesis

Different amounts of NaOH solution with a concentration of 0.1 M were added to the 0.02, 0.01, 0.005 M solutions of Zn(CH₃COO)₂·2H₂O in ethanol. The mixtures were sonicated for 30 min. Different amounts of NaOH solution with a concentration of 0.1 M were added to the 0.02, 0.01, 0.005 M solutions of Zn(CH₃COO)₂·2H₂O in ethanol/water. The obtained mixtures were sonicated for 30-60 min with different ultrasound powers. Table 1, Sample A shows the conditions of reactions in detail. A multi wave ultrasonic generator (BandlinSonopulsGeräte-Typ: UW 3200, Germany) equipped with a converter/transducer and titanium oscillator (horn), 12.5 mm in diameter,

operating at 30 kHz with a maximum power output of 780W, was used for the ultrasonic irradiation. The ultrasonic generator automatically adjusted the power level. The wave amplitude in each experiment was adjusted as needed. The X-ray powder diffraction (XRD) measurements were performed using a Philips diffractometer of X'pert Company with mono chromatized CuK α radiation. The crystallite sizes of the selected samples were estimated using the Sherrer method. The samples were then characterized using a scanning electron microscope (SEM) (Philips XL 30) with gold coating. IR spectra were recorded on a SHIMADZU- IR460 spectrometer in a KBr matrix.

Solvothermal synthesis

Different amounts of NaOH solution with a concentration of 0.1 M were added to the 0.02, 0.01, 0.005 M solutions of Zn(CH₃COO)₂·2H₂O in ethanol. The mixture was stirred vigorously for 30 min and then sealed in a Teflon-lined stainless-steel autoclave. The tank was heated and maintained at 100, 120 and 140 °C for 12 h, and then allowed to cool down to -10 °C temperature rapidly. The product was collected by centrifugation and washed with acetone and ethanol several times to remove the excessive reactants and by products. Then it was calcinated under vacuum at 400 °C for 2 h. The resulting powder was collected for further characterization.

Table 1. Experimental conditions for the preparation of ZnO nanoparticles

Sample A	Zn(OAc) ₂ .2H ₂ O	NaOH	Aging time	Ultrasound power
1	50 mL (0.02 M)	50 mL	30 min	30W
2	50 mL (0.01 M)	50 mL	30 min	30W
3	50 mL (0.005 M)	50 mL	30 min	30W
4	50 mL (0.02 M)	0 mL	30 min	30W
5	50 mL (0.01 M)	0 mL	30 min	30W
6	50 mL (0.005 M)	0 mL	30 min	30W

Sample B	Zn(OAc) ₂ .2H ₂ O	NaOH (0.05 M)	Aging time	Temperature
1	15 mL (0.02 M)	20 mL	12 hr	100 ^{0C}
2	15 mL (0.01 M)	20mL	12 hr	120 ^{0C}
3	15 mL (0.005 M)	20 mL	12 hr	140 ^{0C}
4	15 mL (0.02 M)	0 mL	12 hr	100 ^{0C}
5	15 mL (0.01 M)	0 mL	12 hr	120 ^{0C}
6	15 mL (0.005 M)	0 mL	12 hr	140 ^{0C}

X-ray powder diffraction (XRD) measurements were performed using a Philips diffractometer of X'pert Company with mono chromatized Cuka radiation. The particle sizes of selected samples were estimated using the Sherrer method. The samples were characterized by a scanning electron(SEM) (Philips XL 30) with gold coating. The luminescent properties were investigated using an F-4500 FL spectrophotometer.

Sensing tests

Sensors were made by depositing by drop coating films (1–10 μm thick) of the dispersed in water on alumina substrates (8mm×4mm) with Ptinter digitated electrodes and a Pt heater located on the backside. The structure of the fabricated sensor device has been reported elsewhere [42]. Before sensing tests, a thermal treatment at 400 °C for 2 h was carrying out in order to

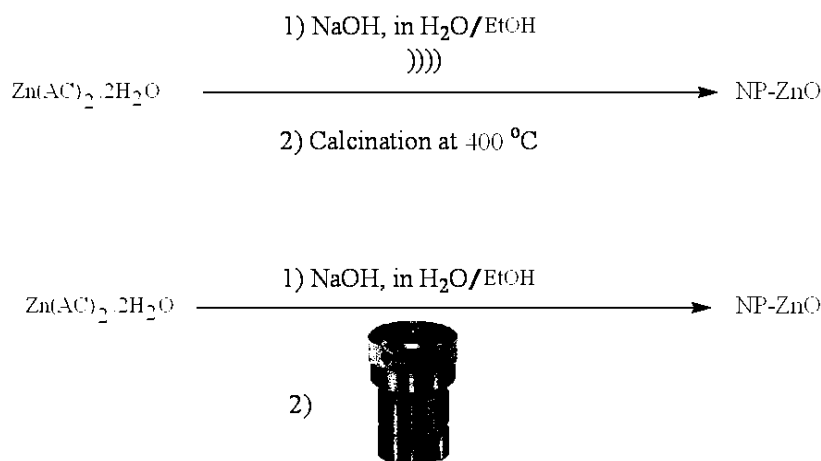
stabilize the microstructure of the sensing film. The sensors were then introduced in a stainless-steel test chamber for the sensing tests. The experimental bench for the electrical characterization of the sensors allows carrying out measurements in controlled atmosphere. Gases coming from certified bottles can be further diluted in air at a given concentration by mass flow controllers. Sensing measurements were carried out in the temperature range from 150 to 400 °C, with steps of 50 °C, under a dry air total stream of 200 sccm, collecting the sensors resistance data in the four point mode. A multimeter data acquisition unit Agilent 34970A was used for this purpose, while a dual-channel power supplier instrument Agilent E3632A was employed to bias the built-in heater of the sensor to perform measurements at super-ambient temperatures. The gas response is defined as the ratio R_{air}/R_{gas} ,

where R_{air} is the electrical resistance of the sensor in dry air and R_{gas} the resistance at different CO_2 concentrations.

Results and discussion

The reaction between zinc acetate and sodium hydroxide to form zinc oxide has been shown in scheme 1. Figure 1 shows the XRD patterns of the ZnO nanoparticles. Figure 1a shows the XRD pattern of the sample that prepared by ultrasonic method before calcination. Figure 1b shows the XRD pattern of the direct sonochemically synthesized ZnO nanoparticles and Figure 1c shows the XRD pattern of the direct solvothermal synthesized ZnO nanoparticles. Figure 1d shows the XRD pattern of the direct sonochemically synthesized ZnO nanoparticles and Figure 1e shows the XRD pattern of the direct solvothermal synthesized ZnO nanoparticles. As it

has been seen the XRD patterns are quite the same and are in agreement with the typical wurtzite structure ZnO diffraction (hexagonal phase, space group $C6v$, with lattice constants $a = 3.24982(9) \text{ \AA}$, $c = 1.6021 \text{ \AA}$, $Z = 2$, JCPDS No.36-1451). Sharp diffraction peaks shown in Figure 1 indicate good crystallinity of ZnO nanoparticles. No characteristic peak related to any impurity was observed. The broadening of the peaks indicated that the particles were of nanometer scale. Estimated from the Sherrer formula, $D = 0.891\lambda/\beta\cos\theta$, where D is the average grain size, λ is the X-ray wavelength (0.15405 nm), and θ and β are the diffraction angle and full-width at half maximum of an observed peak, respectively. The morphology, structure and size of the samples are investigated by Scanning Electron Microscopy (SEM).



Scheme 1. The mechanism of ZnO formation

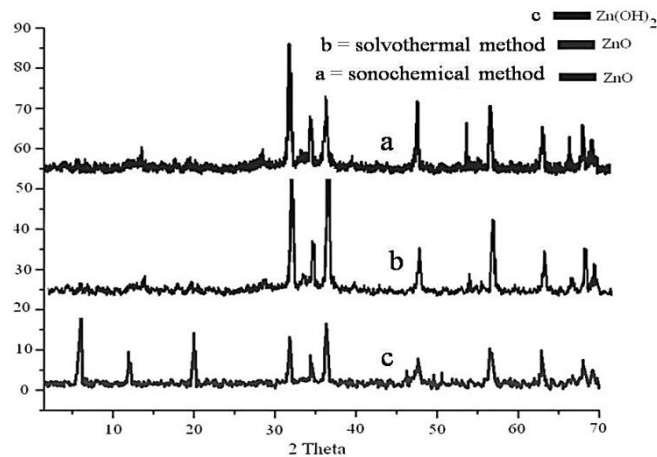


Figure 1. X-Ray powder diffraction pattern of ZnO nanoparticles (a) (sample A. No 2) synthesized by sonochemical method (b) (sample B. No 2) synthesized by solvothermal method, (c) (sample A. No 2) synthesized by sonochemical method before calcinations

Figure 2 indicates that the original morphologies of the ZnO particles are approximately spherical with the diameter varying between 50 to 70 nm for synthesis by sonochemical method (Figure 2a) and 30 to 50 nm for synthesis by solvothermal method (Figure 2b). The average size of the particles of sample A number 2 was 50 nm, and the average size of this sample A after calcination at 400 °C for 4 hours has been calculated about 60 nm which are in agreement with that observed from SEM images. The

average size of the particles of sample B number 2 was 30 nm, which are in agreement with that observed from SEM images. To investigate the size distribution of the nanoparticles, particle size histograms were prepared for the samples A and B, (Figure 3). Most of the particles possess sizes in the range from 40 to 80 nm for sonochemical method and 20 to 60 nm for solvothermal method. For further demonstration, the EDAX was performed for the samples A and B.

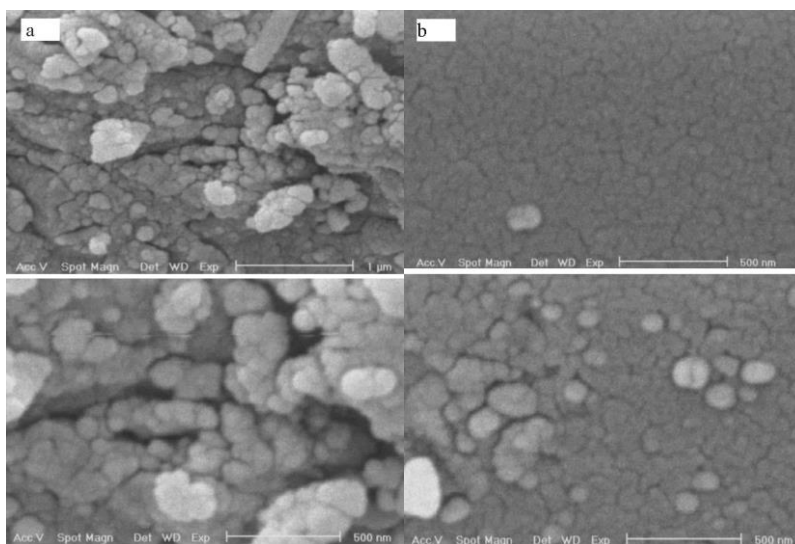


Figure 2. SEM images of ZnO nanoparticles (a) (sample A. No 2) synthesized by Sonochemical method (b) (sample B. No 2) synthesized by solvothermal method

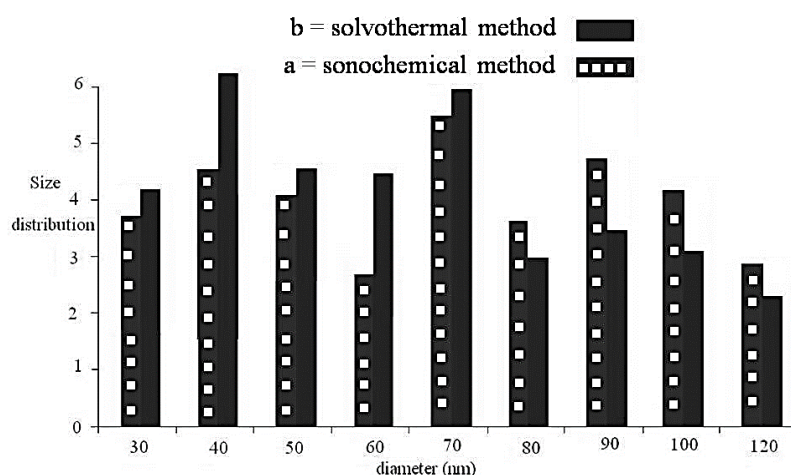


Figure 3. Particle size histograms of ZnO nanoparticles (a) (sample A. No 2) synthesized by sonochemical method (b) (sample B. No 2) synthesized by solvothermal method

The EDAX spectrum in Figure 4 shows the presence of Zn as the only elementary component. In order to investigate the role of sonication on the composition, size and morphology of the products, we carried out the reaction without sonication with the same conditions of the optimized samples. The XRD patterns of the obtained product corresponds to ZnO but the SEM images show that the nanoparticles of the samples without using sonication have larger sizes as compared with the samples obtained via the sonochemical route. It was indicated that the ZnO nanoparticles

could decompose the organic pollutants by formation of exceed superoxide and/or hydroxyl radicals at the ZnO interface in sonochemical method but in solvothermal method the ZnO nanoparticles prepared directly without interface. Figure 5 shows the solid state UV-Vis spectra of the compounds (all ZnOnano powders) display one absorption wide band with the maximum intensity of 376 nm but the solid state UV-Vis spectra of the sample A before calcinations shows two absorption bands in 345 and 360 nm.

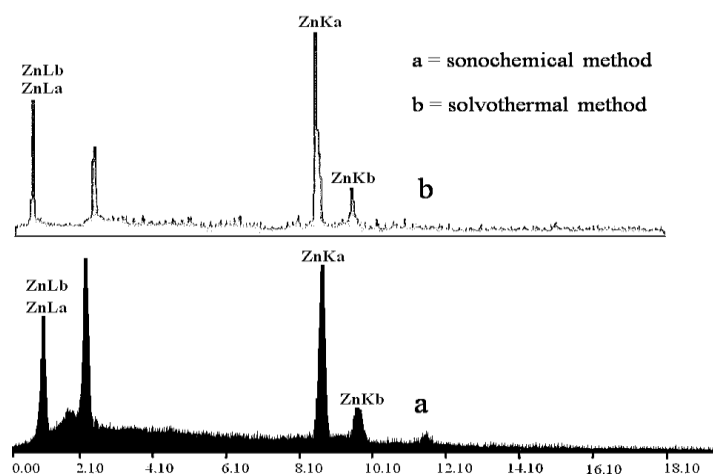


Figure 4. The EDAX analysis of ZnO nanoparticles (a) (sample A. No 2) synthesized by sonochemical method (b) (sample B. No 2) synthesized by solvothermal method

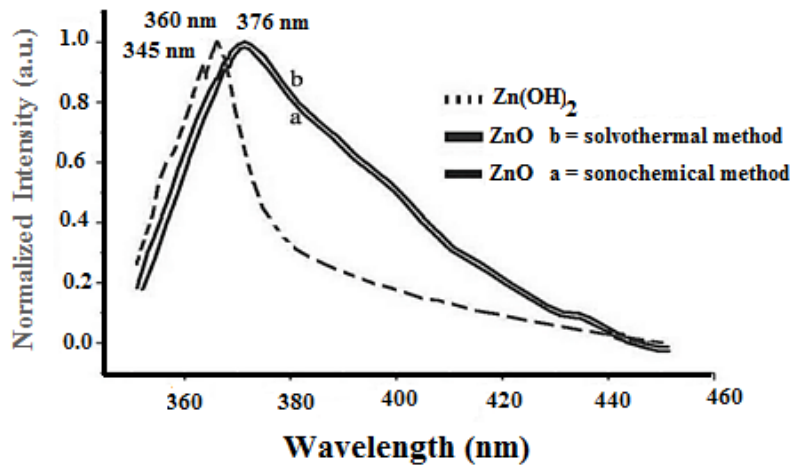


Figure 5. The solid state UV-vis absorption of ZnO nanoparticles (a) (sample A. No 2) synthesized by sonochemical method (b) (sample B. No. 2) synthesized by solvothermal method

Figure 6 shows the PL spectra of ZnO in the nano sized forms ($\lambda_{exc}=360\text{nm}$). All the nanoparticles of ZnO showed a strong and broad emission band centered at 388-390 nm,

and interface product of sample A showed three weak bands at 384, 549 and 570 nm. Raman spectra of ZnO nanoparticles are shown in Figure 7.

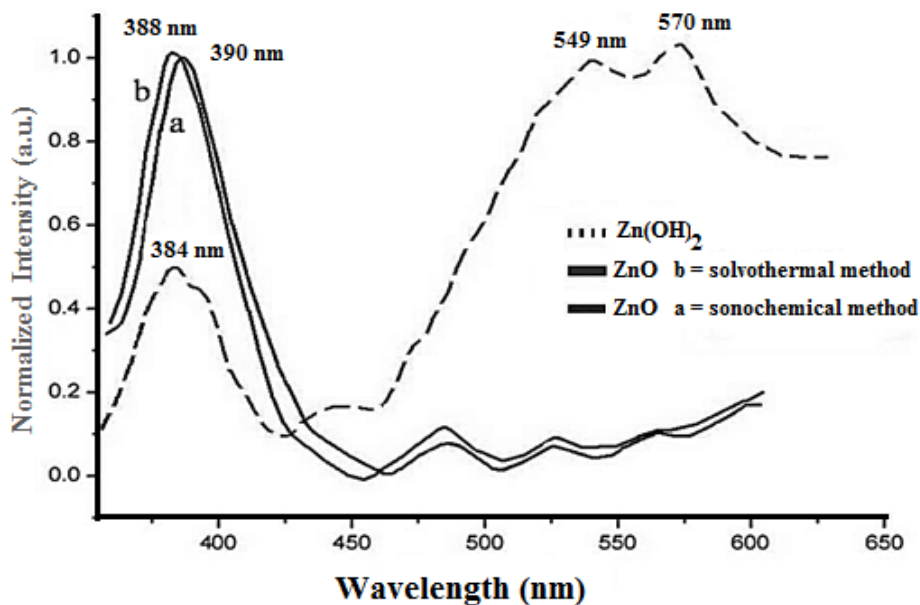


Figure 6. The solid state PL of ZnO nanoparticles (a) (sample A. No. 2) synthesized by sonochemical method (b) (sample B. No. 2) synthesized by solvothermal method

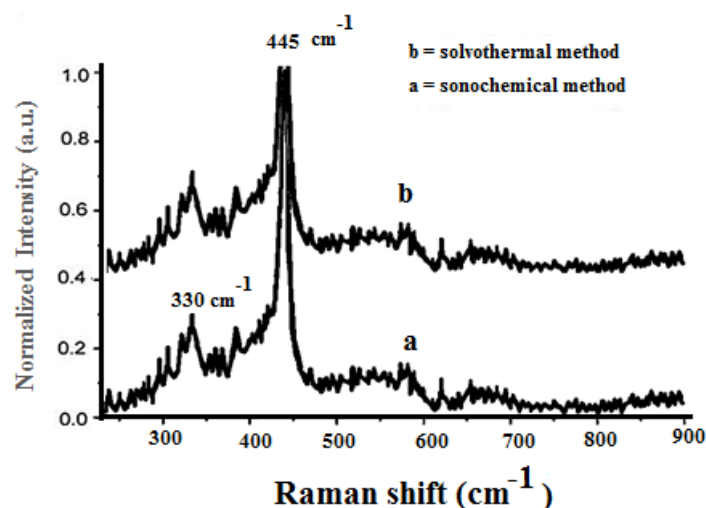


Figure 7. The Raman spectra of ZnO nanoparticles (a) (sample A. No. 2) synthesized by sonochemical method (b) (sample B. No 2) synthesized by solvothermal method

ZnO wurtsit structure shows six Raman active modes. Raman spectra of ZnO nanoparticles show two sharp peaks at 330 and 445 cm^{-1} . This result may be explained by the fact that ZnO nanoparticles have better crystallinity in its nano size form and these emission peaks are virtually the same, indicating that they are influenced by the size of particles. As compared with the other methods used for preparing ZnO nanoparticles. The solvothermal method better than sonochemical method and is very fast and does not need any additives and surfactants during the reactions. The electrical characteristics of the ZnO nanostructures deposited as thick films on alumina substrates have been also investigated. As an example, Figure 8 reports the variation of resistance in the temperature range 25–350 $^{\circ}\text{C}$ for the sample A2 after a heating–cooling cycle in dry air. All prepared films exhibited similar behavior, characterized by a negative temperature coefficient of electrical resistance, which is consistent with a semiconducting-type behavior. At room

temperature the resistance of the as-prepared ZNSON film was very high, and not measurable with a conventional resistance meter. After heating (a), the resistance decreased due to the thermal activation of electron charge carriers. The initial high electrical resistance of the as-prepared sample can be attributed to the water adsorbed during storage at room conditions which causes the formation of hydroxyls on the ZnO surface. They attract electrons from the bulk and become negatively charged and give rise to a positive space charge region leading to a high electrical resistance. On the other hand on the successive cooling cycle (b), the samples displayed lower electrical resistance in all temperature range. This was likely associated to the de-hydroxylation of the surface occurred during the heating cycle. Repeating heating–cooling cycles in dry air, a fully reversible behavior with negligible hysteresis was observed, due to the structural stability of ZnO surface layer in dry air in the temperature range investigated.

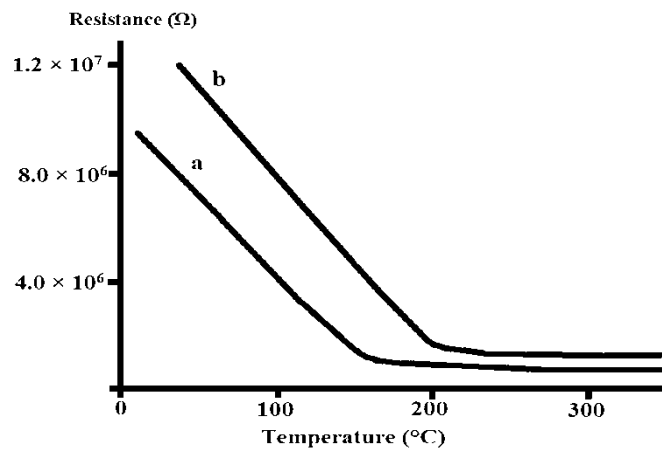


Figure 8. Heating-cooling curves showing the electrical resistance of ZNSON film as a function of temperature

CO sensing tests

It is well known that the response of resistive sensors is highly affected by the operating temperature. Therefore, the response of the ZnO sensors as a function of the operating temperature was first investigated. Figure 9 shows the response as a function of operating temperature from 150 to 400 °C for the ZNSOL sensor exposed to 400 ppm of CO₂. A rapid increase of the response was observed as the working temperature was increased and reached a maximum at about 300 °C and started decreasing thereafter. This characteristic volcano curve can be interpreted on the basis of adsorption-desorption and reaction processes

occurring on the sensing layer surface. For operating temperatures <200 °C the sensor response is low because the adsorbed CO₂ molecules are not activated enough to react with the surface adsorbed oxygen species. However, above 300 °C the decrease in CO₂ gas adsorption is not adequately compensated by the increase of surface reaction and the sensor response decreases. The transient response was found reversible (Figure 10). The response time, τ_{res} , defined here as the time required to achieve 90% of the total resistance change when CO₂ is introduced into air, is fast ($\tau_{res} \sim 25$ s).

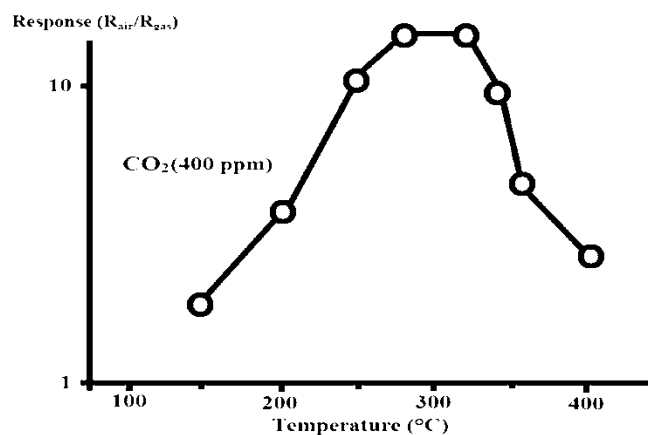


Figure 9. Response to 400 ppm of CO₂ vs. the operating temperature of the ZNSOL sensor

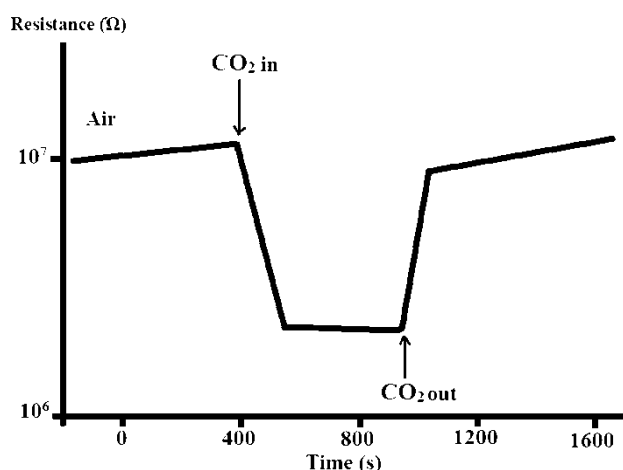


Figure 10. Transient response of ZNSOL sensor to exposure of 100ppm of CO₂ at 300 °C

A slower recovery time, τ_{rec} , i.e. the time required to achieve 90% of the total resistance change when CO₂ is turned off and pure dry air is reintroduced into the chamber has been

observed ($\tau_{res} \sim 150$ s). The response as a function of CO₂ gas concentration for all the ZnO sensors investigated at 300 °C is shown in Figure 11.

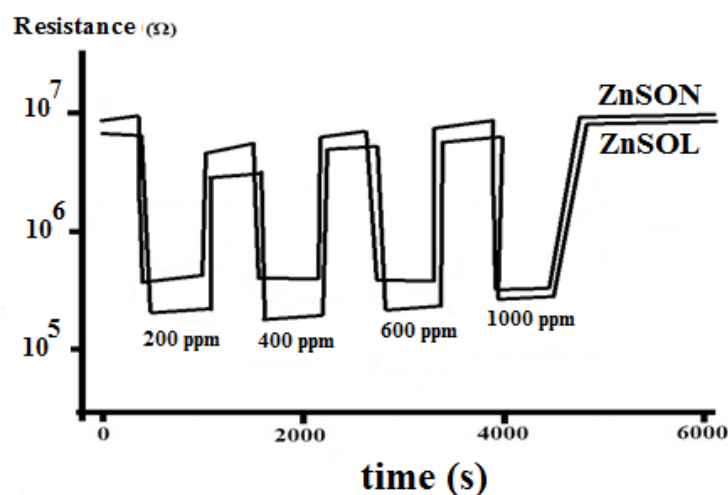


Figure 11. Response to different CO₂ gas concentration for the ZnO sensors at 300 °C

The sensors show a good response to CO₂. The response increased as the CO₂ gas concentration was increased from 100 to 500 ppm. Figure 12a shows the sensor responses vs. CO₂ concentration. A linear trend was observed, when responses are plotted in a log–log scale, as a function of the gas concentration. It is interesting to observe that all the nanostructured films display the same

sensitivity to CO₂, SCO, as calculated by the slope of the extrapolated straight lines reporting the response as a function of the CO₂ concentration in Figure 12b. The sensitivity with respect to CO₂ was calculated to be 0.012 ppm⁻¹. Instead, the responses at a given CO₂ concentration and the detection limits, DL, defined as the lower concentration in which the response

significantly differentiated from the noise signal, i.e. 3 times the standard deviation of noise (instrumental detection limit), are different among the investigated sensors. ZNSOL sensor, based on cloudlike particles, exhibits a slightly greater response than other sensor with various morphology particles, while on ZNSON sensor (nanoparticle) the lower response was found, and the same trend was found for the detection limits. The

extrapolated limit of detection for the ZNSOL sensor is about 0.5 ppm, allowing a monitoring of CO₂ down to concentrations in the sub-ppm range. Even though a direct comparison with recent literature reports on CO₂ sensing of various ZnO nanostructures cannot be made because of the different experimental conditions adopted the results we obtained clearly indicate the good performances of our sensors.

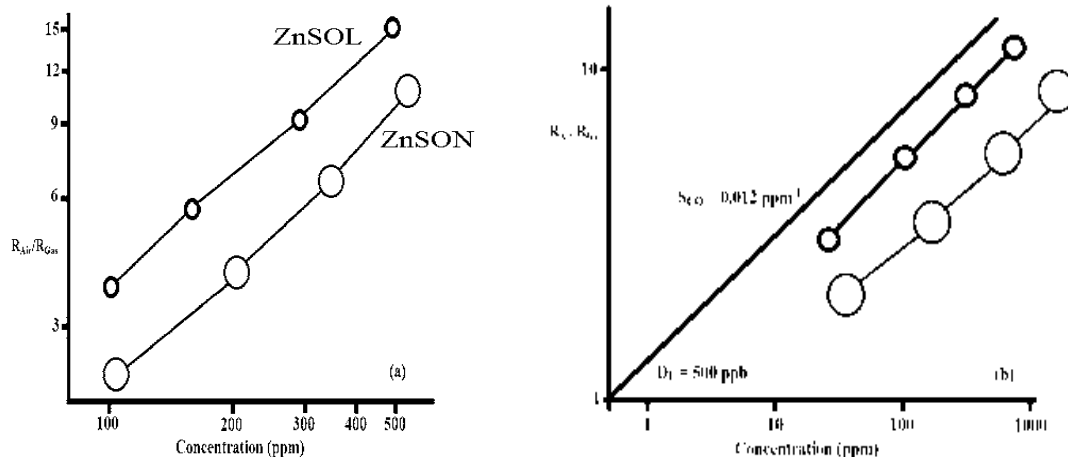


Figure 12. (a) Calibration curves of the ZnO sensors at 300 °C; (b) calibration curves of the ZnO sensors showing the measured sensitivity to CO₂ and the extrapolated detection limit related to ZNSOL sensor

Conclusion

A simple wet chemical process assisted by sonochemical and solvothermal was proposed for the synthesis of different ZnO nanostructures for gas sensing applications. Moreover, by changing the synthesis parameters ZnO nanostructures with different shape/morphology could be obtained. These nanostructures were investigated in the monitoring of carbon dioxide, showing the maximum of response around 300 °C. The higher response was obtained for the ZNSOL sensor based on ZnO nanoparticles exhibiting spherical morphology. A synergic effect between small crystallite size/high surface area and potential barrier modification is proposed for explaining the enhanced sensing

properties of the ZnO particles with spherical morphology. In summary, from this study, it can be deduced that the performance of resistive ZnO based sensors to CO₂ gas can be controlled by tuning the morphology of the metal oxide nanoparticles by a rapid synthesis procedure assisted by solvothermal and sonochemical, providing a simple way to fabricate highly sensitive CO₂ gas sensors. Higher response was obtained for the ZNSOL sensor based on ZnO nanoparticles exhibiting spherical morphology. A synergic effect between small crystallite size/high surface area and potential barrier modification is proposed for explaining the enhanced sensing properties of the ZnO particles with spherical morphology. In summary, from this study, it can be

deduced that the performance of resistive ZnO based sensors to CO₂ gas can be controlled by tuning the morphology of the metal oxide nanoparticles by a rapid synthesis procedure assisted by solvothermal and sonochemical, providing a simple way to fabricate highly sensitive CO₂ gas sensors.

Acknowledgments

Supporting of this investigation by Lorestan University is gratefully acknowledged.

References

- [1] N. Yamazoe, *Sens. Actuators B*, **1991**, 5, 7-19.
- [2] E. Comini, *Analytica Chimica Acta*, **2006**, 568, 28-40.
- [3] N. Bonini, M.C. Carotta, V. Guidi, C. Malagu, G. Martinelli, L. Paglialonga, M. Sacerdoti, *Sens. Actuators B*, **2000**, 68, 274-280.
- [4] E. Comini, G. Sberveglieri, M. Ferroni, V. Guidi, C. Frigeri, D. Boscarino, *J. Mater. Res.*, **2001**, 16, 1559-1564.
- [5] Z.W. Pan, Z.R. Dai, Z.L. Wang, *Science*, **2001**, 291, 1947-1949.
- [6] E. Comini, G. Faglia, G. Sberveglieri, Z. Pan, Z.L. Wang, *Appl. Phys. Lett.*, **2002**, 81, 1869-1871.
- [7] C.B. Murray, C.R. Kagan, M.G. Bawendi, *Annu. Rev. Matter Sci.*, **2006**, 30, 545-610.
- [8] G.-M. Chow, N. IvanovaNoskova, *Nano-structured Materials Science and Technology*, Kluwer Academic Publishers, Dordrecht, **1998**.
- [9] L. Mazzola, *Nat. Biotechnol.*, **2003**, 21, 1137-1143.
- [10] R. Paul, J. Wolfe, P. Hebert, M. Sinkula, *Nat. Biotechnol.*, **2003**, 20, 277-282.
- [11] G. Blaser, T. Ruhl, C. Diehl, M. Ulrich, D. Kohl, *Physica A: Statistical and Theoretical Physics*, **1999**, 266, 218-223.
- [12] G. Korotcenkov, *Sensors and Actuators B*, **2005**, 107, 209-232.
- [13] B. Levy, *Journal of Electroceramics*, **1997**, 1, 239-272.
- [14] J. Bandara, C.M. Divarathne, S.D. Nanayakkara, *Solar Energy Materials and Solar Cells*, **2004**, 81, 429-437.
- [15] J. Bandara, J.P. Yasomane, *Semiconductor Science and Technology*, **2007**, 22, 20-24.
- [16] C.L. Liao, Y.H. Lee, S.T. Chang, K.Z. Fung, *Journal of Power Sources*, **2006**, 158, 1379-1385.
- [17] J. Liqiang, W. Baiq, X. Baifu, L. Shudan, S. Keying, C. Weimin and F. Honggang, *J. Solid State Chem.*, **2004**, 177, 4221-4227.
- [18] V.R. Shinde, T.P. Gujar and C.D. Lokhande, *Sens. Actuators, B*, **2007**, 120, 551-559.
- [19] S.K.N. Ayudhya, P. Tonto, O. Mekasuwandumrong, V. Pavarajarn, P. Praserthdam, *Cryst. Growth Des*, **2006**, 6, 2446-2450.
- [20] M. Vafae, M.S. Ghamsari, *Mater. Lett.*, **2007**, 61, 3265-3268.
- [21] Y.S. Kim, W.P. Tai, S.J. Shu, *Thin Solid Films*, **2005**, 491, 153-160.
- [22] C. Wu, X. Qiao, J. Chen, H. Wang, F. Tan, S. Li, *Mater. Lett.*, **2006**, 60, 1828-1832.
- [23] Xiaochen Sun, Hongzhou Zhang, Jun Xu, Qing Zhao, Rongming Wang and Dapeng Yu., *Solid State Commun.*, **2004**, 129, 803-807.
- [24] P.X. Gao, Z.L. Wang, *Appl. Phys. Lett.*, **2004**, 84, 2883-2885.
- [25] L. Vayssieres, *Adv. Mater*, **2003**, 15, 464-466.
- [26] C.H. Liu, J.A. Zapien, Y. Yao, X.M. Meng, C.S. Lee, S.S. Fan, Y. Lifshitz, S.T. Lee, *Adv. Mater*, **2003**, 15, 838-841.
- [27] H. Zhang, X.Y. Ma, J. Xu, J. Niu and D. Yang, *Nanotechnology*, **2003**, 14, 423-426.

- [28] Y. Liu, J. Zhou, A. Larbot, M. Persin, J. *Mater. Process. Technol.*, **2007**, 189, 379-383.
- [29] Z. Fan, D. Wang, P. Chan, W. Tseng, J.G. Lu, *App. Phys. Lett.*, **2004**, 84, 5925-5931.
- [30] Z. Fan, J.G. Lu, *Appl. Phys. Lett.*, **2005**, 86, 032111-3.
- [31] Z. Fan, J.G. Lu, *Appl. Phys. Lett.*, **2005**, 86, 123510-3.
- [32] X. Wen, W. Zhang, S. Yang, Z.R. Dai, Z.L. Wang, *Nano. Lett.*, **2002**, 2, 1397-1401.
- [33] Y. Chang, H.C. Zeng, *Cryst. Growth Des.*, **2004**, 4, 397-402.
- [34] G.H. Yue, P.X. Yan, D. Yan, J.Z. Liu, D.M. Qu, Q. Yang, X.Y. Fan, J. *Crystal Growth*, **2006**, 293, 428-432.
- [35] J.Q. Hu, Y. Bando, J.H. Zhan, Y.B. Li, T. Sekiguchi, *Appl. Phys. Lett.*, **2003**, 83, 4414-4416.
- [36] J.J. Wang, M.Y. Zhu, R.A. Outlaw, X. Zhao, D.M. Manos, B.C. Holloway, V.P. Mammana, *Appl. Phys. Lett.*, **2004**, 85, 1265-1267.
- [37] J. Ghijsen, L.H. Tjeng, J. van Elp, H. Eskes, J. Westerink, G.A. Sawatzky, M.T. Czyzyk, *Phys. Rev. B*, **1988**, 38, 11322-11330.
- [38] D. Wu, Q. Zhang, M. Tao, *Phys. Rev. B*, **2006**, 73, 235.
- [39] H. Yamada, X.G. Zheng, Y. Soejima, M. Kawaminami, *Phys. Rev. B*, **2004**, 69, 104104-1-7.
- [40] X.G. Zheng, Y. Kodama, K. Saito, E. Tanaka, Y. Tomokiyo, H. Yamada, C.N. Xu, *Phys. Rev. B*, **2004**, 69, 094510-0945105.
- [41] A. Chowdhuri, P. Sharma, V. Gupta, K. Sreenivas, K.V. Rao, *J. Appl. Phys.*, **2002**, 92, 2172-2180.
- [42] G. Neri, A. Bonavita, G. Micali, G. Rizzo, E. Callone, G. Carturan, *Sens. Actuators B*, **2008**, 132, 224-233.